Energy Storage Materials 76 (2025) 104115

Contents lists available at ScienceDirect

Energy Storage Materials

journal homepage: www.elsevier.com/locate/ensm

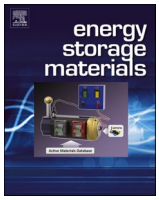

Supercapacitor safety: Temperature driven instability and failure of electrochemical double layer capacitors

Katrina Mazloomian [a,1], Thomas R. Dore [a,1], Mark Buckwell [a,c], Liam Bird [a,b,d], Paul R. Shearing [b,d], Thomas S. Miller [a,b,*]

[a] Electrochemical Innovation Lab, Department of Chemical Engineering, University College London, London, WC1E 7JE, UK
[b] The Faraday Institution, Quad One, Harwell Science and Innovation Campus, Didcot OX11 0RA, UK
[c] Advanced Propulsion Lab, Marshgate, University College London, London E20 2AE, UK
[d] The ZERO Institute, University of Oxford, Holywell House, Osney Mead, Oxford, OX2 0ES, UK

ARTICLE INFO

Keywords:
EDLC
Ultracapacitor
Overcharge
Overheating
Abuse testing

ABSTRACT

While supercapacitors are widely considered to be safer than current lithium-ion battery technologies, their reputation for safety, stability, and long cycling lifetimes is primarily based on their testing under highly favourable electrochemical and environmental conditions. However, the impact of extreme conditions on even the most common Electrochemical Double Layer Capacitors (EDLCs) remains unclear, limiting the understanding of their potential failure mechanisms and the risks they could present to individuals and systems into which they are increasingly being integrated. In this study, we investigate the effects of thermal abuse conditions, induced by overheating and overcharging, on a typical commercial EDLC. Our findings reveal that while EDLC cell failures are less extreme than the well-documented failures of Li-ion batteries, they still pose significant risks to the integrity of the cell itself and the direct environment. This is most evident from the fact that between the overheating and overcharging tests, more than half of all the cells tested in this study failed catastrophically, leading to an explosive event. The high cell temperatures induced by these abusive tests led to electrolyte vaporisation and cell gassing that was not effectively mitigated by cell vent designs. This study therefore challenges the perception of intrinsic supercapacitor safety and provides a foundation onto which safer system designs can be built.

1. Introduction

Supercapacitors are an important energy storage technology that have gained traction due to their high-power density, rapid charge/discharge capability, and long cycle lifetimes compared to traditional batteries. The application of supercapacitors across the automotive, aerospace, medical and personal electronics sectors is driving the growth of their global market. For instance, supercapacitors can be combined with batteries in vehicles to improve regenerative braking systems [1], or integrated with combustion engines in hybrid vehicles [2]. However, including supercapacitors in such applications exposes them to significant risks, including vehicle fires and crashes, as well as exposure to a variety of challenging environmental conditions, such as high temperatures. Hence, it is crucial to understand the safety and behaviour of supercapacitors under potential failure scenarios.

Abuse testing simulates conditions of intentional misuse to study the response of electrochemical cells. Supercapacitors could experience overcharging due to inadequate charging control or electrical malfunctions and overheating during extreme weather conditions or vehicle fires. Yet while extensive studies have examined the effects of various failure scenarios on batteries [3–8], leading to well-established industrial standards for these devices [9–12], supercapacitors have been rarely examined [13], beyond aging and performance studies [14–16]. Currently, safety standards and regulations for integrating supercapacitors into electronic devices and systems are highly application-specific, focusing more on implementation, electrical integration, and transport criteria rather than the intrinsic safety of the supercapacitor devices themselves. None offer a comprehensive standard for safe supercapacitor application. Despite sharing some commonalities with batteries, supercapacitors have distinct chemistry,

* Corresponding author.
1 Equal contribution.
E-mail address: t.miller@ucl.ac.uk (T.S. Miller).

https://doi.org/10.1016/j.ensm.2025.104115
Received 15 October 2024; Received in revised form 30 January 2025; Accepted 9 February 2025
Available online 10 February 2025
2405-8297/© 2025 The Author(s). Published by Elsevier B.V. This is an open access article under the CC BY license (http://creativecommons.org/licenses/by/4.0/).

construction, and electrical characteristics, necessitating a dedicated discussion to address their unique safety requirements.

Nonetheless, while studies into supercapacitor safety are few in number, some attempts have been made to address this gap in research. For example, Walden et al. [17] investigated the criteria used for Li-ion batteries, adapting safety standards for rechargeable batteries to target the unique qualities of supercapacitor technology. Elsewhere, studies have examined the performance of Li-ion hybrid capacitors under various conditions. Bolufawi et al. [18] investigated the swelling and gassing of a 200 F Li-ion capacitor pouch cell under overcharge abuse conditions, finding that most failures involved electrolyte decomposition due to temperature increases. This heating triggered exothermic reactions that can lead to swelling, gassing, thermal runaway, and fire. Additionally, Wu et al. [19] observed the thermal response of Li-ion supercapacitor cells to overheating, showing that they underwent thermal runaway processes akin to that seen in the thermal failure of Li-ion batteries. This commonality likely stems from the similarities in their structural and chemical compositions.

Unfortunately, the Li-ion capacitors studied differ significantly from typical EDLCs, the most common type of supercapacitor. Li-ion capacitors integrate elements of Li-ion battery chemistry into supercapacitor structures, commonly pairing a standard supercapacitor electrode, like high surface area carbon, with an electrode that undergoes faradaic energy storage reactions similar to those in Li-ion batteries. This contrasts the typical construction of EDLCs which typically store charge electrostatically using a pair of symmetric carbon electrodes. This raises important questions about the effects of abuse testing on EDLCs, as the differences in chemistries, and fundamental charge storage mechanisms, could drastically alter the impact of abusive conditions. Therefore, specifically studying EDLC failure is essential to understand their unique responses and enhancing their safety and reliability in various applications.

A very limited number of studies specifically address EDLC supercapacitor abuse and safety testing. Most notable is the research by Hund et al. [20] under the U.S. Department of Energy's Energy Storage Program. This study focuses on gases released from acetonitrile-based EDLCs during overcharge and overheating, identifying hazards like acetonitrile, carbon dioxide, and trace amounts of hydrogen cyanide. While the study highlighted the potential for cell failure, emphasising the dangers of hot flammable gas release, its scope was limited by the small sample size and the absence of an in-depth post-mortem analysis. Furthermore, the study did not evaluate the overall impact of failure on cell structure, detailed failure processes, post-failure cell conditions, nor the underlying failure mechanisms. Thus, further studies are required to provide a comprehensive understanding of the failure effects and mechanisms of different abusive conditions on EDLCs, as understanding these aspects of cell failure is vital for ensuring the safe use of these devices and guiding the development of future EDLC designs.

There are also few computational studies evaluating supercapacitor conditions through theoretical models. For instance, Sakka et al. [21] applied theoretical modelling to heat management in EDLC supercapacitor modules for vehicle applications, developing models to predict thermal behaviour. This study examined thermal distribution in cylindrical cells using electrical demands during driving cycles and highlighted the importance of effective heat dissipation for supercapacitor performance and longevity, demonstrating the formation of thermal hotspots within the cell centre. However, it did not consider temperatures beyond typical operational ranges or potential failure effects under extreme conditions, such as a malfunction in the vehicle's charging control circuitry or exposure to significant heat. These effects are difficult to model accurately due to the lack of experimental data needed to create such theoretical models.

The limited understanding of supercapacitor failure represents a significant gap in the literature, with critical safety implications. While it is reasonable to assume that supercapacitor manufacturers are aware of potential hazards and have likely conducted safety testing to meet electrical safety regulations, such data is not publicly accessible and likely focuses on the overall device performance rather than detailed material-level effects. As a result, the impacts of extreme conditions on cell structures, material components, and importantly failure mechanisms remain largely unexamined. This lack of information hinders the development and refinement of studies and predictive models.

Therefore, in our study we uncover important mechanisms of EDLC failure at high temperatures either induced externally or internally (through overcharging). Through a 'whole cell' and multi-length scale approach we reveal the impact of abusive conditions on EDLC cells, and the interplay between material degradation and device failure. This provides a comprehensive understanding of supercapacitor safety and identifying important vulnerabilities in EDLC systems to inform the future development of safer EDLC designs to reduce the risk of failure events.

2. Methods

All abuse tests were conducted in fire-proof chambers equipped with air vents and BOFA extraction systems to contain potential failures, including explosions and gas releases. The primary chamber was the MSK-800-TE9002 (MTI corporation) pneumatic nail penetration tester (Figure SI-1a), with additional overcharging tests performed in the HEL BTC130 (HEL Group). Although a different chamber was used for these tests, the experimental conditions remained consistent, ensuring comparable results.

Within the chambers, the cells were positioned between superwool insulation (Figure SI-1c) and connected to four thermocouples (Figure SI-1b), an IviumStat potentiostat with a 10012 booster (100 A, 12 V maximum), and two rod heaters which were held parallel to the cell length. Each cell was fully charged to 3 V before testing, with temperature, voltage, and current recorded throughout. Overheating tests involved gradually increasing the heater voltage by 1 V every 30 s to a maximum of 60 V at which they were then held, while overcharge tests applied a constant current of 4.2 A without a voltage limit. Both abuse methods had no set time limit and were continued until cell failure.

Postmortem analysis of the cells involved a multi-length scale characterisation to assess the effects of the abuse tests. X-ray CT was conducted using a Nikon XT H 225 system (Nikon Metrology, Japan) to capture large-scale damage across the entire cell prior to disassembly. Subsequently, scanning electron microscopy (SEM) was performed on a Zeiss UltraPlus analytical field emission SEM (FESEM), equipped with an Oxford Instruments INCAx-act energy-dispersive X-ray analysis (EDX) system (10 mm^2 Silicon Drift Detector, ATW 129 eV), to investigate microstructural changes. Additionally, Raman spectroscopy was carried out using a Renishaw inVia micro-Raman spectrometer to further assess the chemical and structural degradation.

A more detailed description of the experimental setup and procedures employed within this study is provided in the SI.

3. Results

Abuse testing involves subjecting cells to conditions that exceed their standard operating parameters. This study specifically focuses on overheating and overcharging abuse testing of EDLC supercapacitors. Fig. 1 depicts the characterisation of a pristine cell, providing insight into both the structural and material composition of the pristine supercapacitor cell, vital information to enable comparative pre- and post-mortem analysis.

X-ray CT allows for non-destructive visualisation of the internal structure and components of supercapacitor cells, and can be used to reveal internal defects, structural integrity, and can showcase the overall architecture without disassembling the cell. Fig. 1a shows a typical X-ray CT view of a 'pristine' cell, illustrating the uniform electrode layer spacing. The X-ray images are presented in greyscale based on the X-ray absorption coefficient of the material, with higher attenuating materials

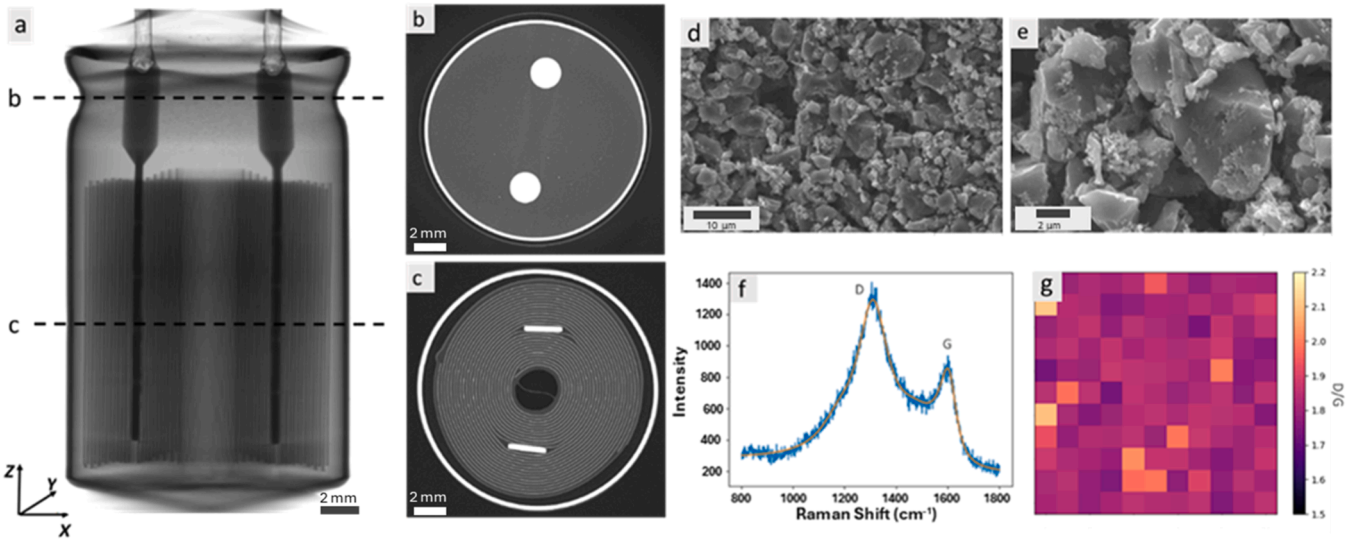

Fig. 1. Pristine cell characterisation. X-ray CT images showing a) the full cell, as well as orthoslices in the XY plane of the b) rubber cap and c) a representative view of the electrode coil as it appears throughout the length of the cell. SEM images of the pristine cell electrodes are shown at magnifications of d) 5 K and e) 15 K. f) Raman point spectrum of the pristine carbon electrode from 800 to 1800 cm^{-1}. Raw data is presented in blue and the fitting in orange. g) Raman map of the ratio of the intensities of the D and G peaks (D/G) for the pristine carbon electrode over a 100 × 100 μm^2 area consisting of 121 individual point spectra.

appearing brighter and less attenuating materials appearing darker. The pins used for electrical connections are also clearly visible in the cross-sectional image through the cell cap (Fig. 1b). The electrodes, primarily composed of carbon compounds, appear darker, but individual layers are distinguishable in the cross-sectional image of the coil (Fig. 1c). Scans on all cells tested in this study were performed prior to destruction, and additional representative images are shown in Figure SI - 2 and Figure SI - 3. All pristine scans yielded nearly identical results, with visual inspections revealing no major defects or manufacturing faults that could have influenced or exacerbated the cells' response to abuse conditions.

After cell disassembly, SEM imaging of representative areas from electrodes extracted from pristine cells allowed for direct visualisation of the electrode surfaces, and revealed non-uniform, amorphous carbon particles embedded in a larger carbon binder framework, likely indicative of activated carbon[22] (Fig. 1d-e). This was confirmed using EDS and X-ray photoelectron spectroscopy (XPS), which showed identical elemental composition in both electrodes, indicating cell symmetry as expected (Figure SI - 4a-d). Traces of fluorine, nitrogen, and boron were also noted, suggesting the electrolyte salt was $TEABF_4$, a salt commonly used in conjunction with an acetonitrile solvent. The presence of acetonitrile solvent was confirmed via mass spectrometry (Figure SI - 4e).

A characteristic Raman spectrum of the pristine electrode obtained from 800 to 1800 cm^{-1} is shown in Fig. 1f, focusing on the characteristic carbon features. A Raman map produced from 121 individual point spectra over a 100 × 100 μm area indicated a D/G ratio consistently greater than 1, with an average value of 1.9, characteristic of high surface area disordered carbon [23]. This conclusion is further supported by the extended range Raman spectra shown in Figure SI - 5, which reveals the absence of a 2D peak—a characteristic feature of graphitic carbon. Its absence, in addition to the large D peak, highlights the amorphous and disordered nature of the carbon electrodes. The map also demonstrates the homogenous behaviour of the surface as only minor fluctuations of the D/G ratio are observed.

Charge/discharge cycling tests of the cell showed stable performance over 600,000 cycles, as illustrated in Figure SI - 4f, which plots capacitance values for the first of every 100 cycles. The capacitance dropped from an initial value of 25.05 F to 23.2 F within the first 3000 cycles, then stabilised at approximately 21 F (84 % of the initial value), maintaining this value for the duration of the testing period. This demonstrates the cell's long cycle life and absence of major early-onset calendar aging.

These material characterisations reveal that the cells examined in this study consist of an electrode coil made of high-surface-area carbon deposited on aluminium current collectors, paired with a paper separator. The separator is wetted with an acetonitrile-based electrolyte containing the ionic salt TEABF4, representing a standard composition and structure typical of EDLC supercapacitors.

3.1. *Overheating*

While these EDLCs have been shown to be consistent in their manufacturing and demonstrated to perform as expected under standard operating conditions, changes in environmental temperatures have been shown to influence supercapacitor performance [24], as elevated temperatures enhance mass transport and improving kinetics within electrochemical cells, thereby increasing the power density. However, excessive heat can surpass the activation energy barrier for decomposition reactions [25,26], causing the breakdown and vaporisation of the electrolyte. This gassing process, extensively detailed in battery failure literature, can lead to pressure buildups within cells, resulting in potential hazards such as cell rupture, release of hazardous gases, explosions, and potentially fires. In contrast the effects of extreme temperatures beyond the operational limits of supercapacitors have not been sufficiently investigated. Given the known sensitivity of supercapacitors to temperature fluctuations, a thorough understanding of their thermal resilience during operation is essential.

Overheating tests were conducted at 100 % SOC to simulate and characterise the behaviour of the cells under extreme temperatures, by replicating conditions that could arise from external heat sources such as a nearby fire, faulty thermal management systems, or excessive ambient heat. The effects of this abuse are presented for five EDLC cells, referred to as OH_1 through OH_5.

Overheating abuse of these EDLCs testing using external heating resulted in two distinct outcomes. The first, illustrated in Fig. 2, is characterised by elevated temperatures accelerating a progressive decline in cell voltage beyond the typical self-discharge rate observed under ambient conditions. Typically, the cells maintained a voltage of 2.7 V even after an hour of operation (Figure SI - 6a). However, at

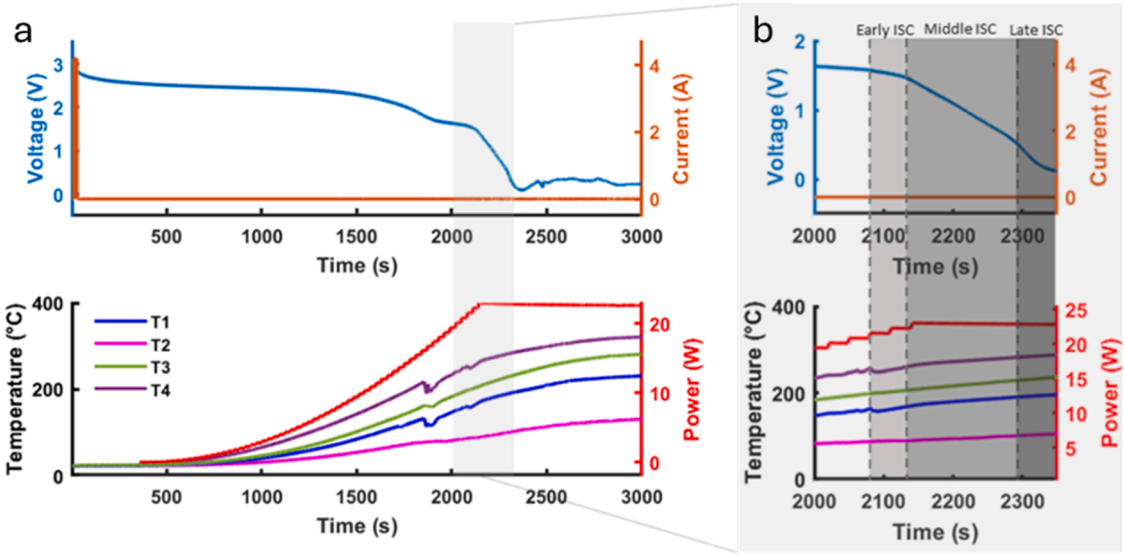

Fig. 2. Overheating Cell OH_1. a) The top plot displays voltage (V, blue) and current (A, orange) profiles, while the bottom plot presents thermocouple and heater data (W, red). b) Inset of the cell behaviour from $t = 2000$ s to $t = 2350$ s that reveals distinct phases of early ISC (light grey), middle ISC (darker grey), and late ISC (darkest grey).

elevated temperatures ranging from 50 to 150 °C, there is a significant and continuous voltage drop, indicating early signs of failure. Cells OH_1, OH_2, and OH_4 exhibited consistent responses to increasing temperatures. A notable observation, illustrated in Fig. 2a, is the simultaneous drop in both voltage and temperature at ~1800 s. This phenomenon can be attributed to the release of gaseous decomposition products, evidenced by observations of gaseous vapour emanating from the cells.

At this point, the high external cell temperatures exceeded 150 °C, far surpassing the boiling point of acetonitrile [27], which led to the vaporisation and decomposition of the electrolyte. This caused internal pressure to rise beyond the cell's structural tolerance. This overpressure triggered the activation of the vent, a standard safety feature often utilised in commercial supercapacitor cells, which allowed for the release of gaseous products to prevent catastrophic failure [25], by offering a more controlled failure mechanism. For the cells used in this study, the vent is positioned on the bottom face (Figure SI - 6b). Once this vent ruptures, the cell is rendered damaged and unusable.

Further heating of the cells led to the destruction of the separator as the temperature exceeded the decomposition point of common separator materials. This triggered an internal short circuit (ISC), the evolution of which Lai et al. [28] have described for Li-ion batteries in three stages: Early, Middle, and Late ISC. This theory can be extended to explain the behaviour observed for these supercapacitors and has been highlighted in the inset of Fig. 2b.

- ***Early ISC:*** The separator material begins to break down, causing the pores in the separator to close due to the decomposition of the material itself or any additives/coatings. This increases the internal resistance of the cell, leading to a slow drop in cell voltage.
- ***Middle ISC:*** The separator continues to degrade as the temperature within the cell rises. This degradation reduces the ISC resistance, causing a noticeable decrease in cell voltage. When the separator reaches its failure temperature, it begins to char and may degrade either completely or enough to allow the opposing electrodes to make localised contact.
- ***Late ISC:*** Extensive contact occurs between the anode and cathode materials. This results in a significant internal short circuit and an inevitable drop in voltage down to ~ 0 V.

These observed patterns were consistent across two additional cells (OH_2, and OH_4) that experienced overheating, as evidenced by the data obtained from Cell OH_2 (Figure SI - 6c).

Importantly, of the five cells tested, two cells exhibited significant deviations from the aforementioned pattern, violently rupturing within 30 mins of heating. This rupture expelled the rubber cap from the outer aluminium casing and ejected the internal components, resulting in the deformation and detachment of the pins from the fragmented electrode remnants. Fig. 3 illustrates this failure, presenting the electrochemical and thermal data for cell OH_3 and demonstrating the abrupt nature of cell failure at temperatures comparable to the venting process observed in other overheated cells (cell temperatures: T1 = 126 °C, T3 = 150 °C).

The explosive failures of cells OH_3 and OH_5 account for a substantial proportion (40 %) of the tested cells. Although a larger sample size would provide greater statistical significance, the results underscore the efficacy of the testing methods and highlight possible risks associated with these devices. The energetic destruction observed could pose hazards to individuals and surrounding components due to the release of hot flammable gases, shards, and potential fire hazards. Importantly, this divergence in failure cannot be attributed to the testing procedures, as all tests were conducted under nominally identical conditions.

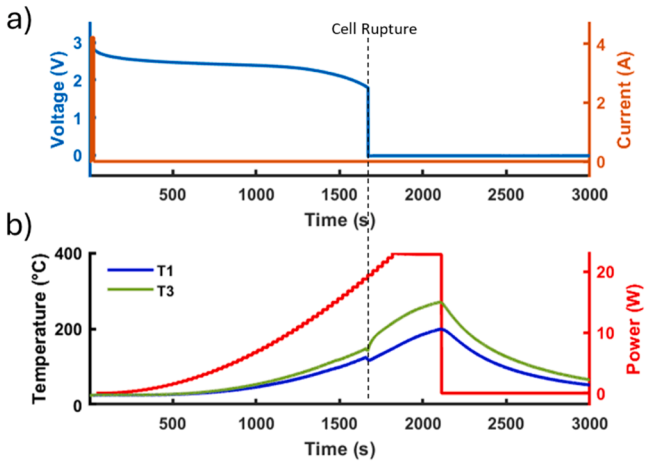

Fig. 3. Overheating Cell OH_3. Electrochemical and thermal data showing an explosive event at 1660 s. a) Plot displays voltage (V, Blue) and current (A, Orange) profiles, while b) presents thermocouple and heater data (W, red).

Furthermore, X-ray CT scans revealed no apparent defects in any of the tested cells prior to abuse. However, this does not exclude the possibility of variations in quality control measures or the existence of internal defects, such as impurities in the electrodes or separators, or structural abnormalities that may not be detectable at the resolution of the X-ray CT scans, which could render some cells more susceptible to failure.

Despite the divergence in the final outcomes, the exploded cells exhibited an electrochemical/thermal response very similar to the non-exploded cells during the initial heating stages. This is showcased in the voltage profile for OH_3 which shows a comparable pattern of self-discharge to that of OH_1 and OH_2 ('Vented cells'), this is concerning as there appeared to be little identifiable warning of the pending catastrophic failure. This trend continued until the point where OH_1 and OH_2 vented; however, the voltage profile for OH_3 (Fig. 3) lacks the indicative temperature drop caused by the venting process. Thereby suggesting that the venting mechanism for OH_3 may have malfunctioned during operation, preventing the discharge of vapours and alleviation of pressure within the cell. As the accumulation of vapours intensified, the pressure reached a critical threshold, causing the outer casing to rupture and leading to an explosive event. This is indicated by a complete and sudden loss of voltage at approximately 1660 s, coinciding with a slight drop in temperature. Furthermore, no gas emissions were observed prior to the rupture of Cell OH_3.

After the cell failure, the temperature profiles show a persistent increase as the heaters climbed to their final power. Upon shutdown of the heaters, an immediate temperature decline was observed. It is important to note that the temperature measurements following the rupture event are unlikely to be entirely reliable due to the detachment of the thermocouples from the cell and the compromised integrity of the cell itself. Temperature measurements for this experiment are reported only for T1 and T3, as T2 and T4 malfunctioned during the cell explosion.

The overheating tests therefore revealed that electrolyte vaporisation and subsequent pressure build-up could trigger EDLC cell failures at temperatures approaching 200 °C. Although such extreme temperatures are unlikely during normal operations, they could occur during fires or due to the failure of nearby electrochemical devices, such as Li-ion batteries experiencing thermal runaway. Both failure outcomes pose significant risks, as whilst cell explosions present direct safety risks, including physical injury, damage to electronic devices or vehicles, and environmental harm from hazardous chemicals, the venting process whilst also releasing hazardous chemicals, it also releases hot, highly flammable gases that could ignite or worsen a pre-existing fire. Therefore, addressing these risks is crucial when considering the safety and application of these devices.

Addressing these hazards is challenging due to the inconsistency in failure responses, which complicates the accurate prediction and implementation of necessary safety measures for these devices. While the failure mechanisms resulting from thermal abuse during overheating tests has been identified, pinpointing the underlying factors that determine whether catastrophic failure or venting occurs is more difficult. It is therefore suggested that a combination of potential factors may influence whether the cells 'exploded'. These factors may include experimental variables, such as the positioning of the electrode coil within the cell, minor differences in testing conditions, discrepancies in thermal distribution across the cells. In addition to manufacturing considerations, such as defective or deficient vent systems that are unsuitable for conditions beyond the cells' typical operating parameters.

Visual inspections of the failed cells confirmed a key distinction between the exploded and non-exploded cells. In each of the non-exploded cells, the vent region had expanded and was accompanied by the presence of a black residue near the vent opening (Figure SI - 6d). This substance is likely residual electrolyte that underwent combustion, leaked out, and dried around the vent. Furthermore, the rubber cap located at the top of the cell, where the two terminals protrude, was displaced outward due to pressure build-up, and showed signs of burning and disintegration (Figure SI - 6(e-f)). In contrast, the exploded cells showed none of these indicators, as their vents failed to open. This resulted in cell rupture before they could undergo a prolonged period of elevated temperatures that would have caused further degradation.

Post-mortem characterisation, as presented in Fig. 4, was carried out on the overheated cells to assess the effects of prolonged exposure to elevated temperatures in comparison to their initial pristine state. X-ray CT allowed for a comprehensive visualisation of the failed cells, however, was not feasible for the remains of the exploded cells (OH_3 and OH_5), as their interiors were ejected, leaving only empty casings. X-ray analysis, coupled with surface level analysis of the electrodes via Raman spectroscopy, provided detailed insights into the structural and chemical alterations induced by the abuse tests, facilitating a thorough understanding of the failure mechanisms in supercapacitors.

The X-ray CT images in Fig. 4 show a full-cell, post-mortem image of Cell OH_4, including several orthoslices (b, c, d, and e) captured in the XY plane, which runs parallel to the direction of the pins. These images indicate that overheating-induced failures were evenly dispersed throughout the cell structure. Notable signs include kinks and bends in the electrode layers, unbound carbonaceous material spread throughout, and evidence of excessive pressure affecting the cell casing's integrity. The pins themselves show significant structural damage, such as bending and deformation, posing a problem due to their attachment to the electrodes and their tightly wound configuration within the coil. Movement of these structures can lead to bending or stretching of the electrodes along their entire length, exerting strain on both individual particles and the bulk material within the coil. These effects were consistent with the other non-exploded overheated cells, especially in OH_1 (shown in Figure SI - 7), where the electrode coil had shifted off-centre compared to the pristine cell configuration due to excessive debris and disintegrated electrode material, collectively contributing to increased disorder within the cell.

As previously mentioned, 'vented cells' displayed visible expansion on their lower surface near the vent. The profile in Fig. 4a reveals that the vent of Cell OH_4 ruptured, causing a protrusion of approximately 1.9 mm. Other overheated cells that did not explode had expanded vent caps (OH_1 and OH_2). This suggests that the venting mechanism effectively functioned in three out of the five tested cells by facilitating the gradual release of gaseous vapours and preventing explosive events. The various orthoslices in Fig. 4b-e show the effects of failure throughout the cell's length. Fig. 4b indicates that the rubber cap degraded and combusted, resulting in fragmentation, cracking, and disintegration. These processes rendered the cap more permeable, potentially aiding gas release for sufficient venting. Significant void areas were observed near the pins, suggesting that the aluminium may have functioned as a heat sink, retaining the heat within more localised regions and thereby accelerating degradation in those areas.

At the top of the electrode coil (Fig. 4c), the coil was forced into an oval shape, creating disorder within the cell due to elongation and deformation within the carbon coating of the electrode material. This deformation is attributed to the central void within the cell and the accumulation of substantial charred loose carbonaceous material around the coil's outer edge, which allowed for more observable deformation as the electrodes are pressured inwards. This material could be remnants of the rubber cap, detached electrode material, or carbonised separator products. Additionally, this build-up of loose material is further observed in Fig. 4e at the cell's bottom.

The orthoslice in Fig. 4d reveals points where the coil disengaged from the aluminium pins, creating irregular electrode layer spacing and potentially undermining ionic conductivity and overall device capacity. Jagged bends in the electrode indicate localised strain with unbound carbon material accumulating near the pins reflecting an irreversible loss of capacity. Frayed edges on the coil's exterior and ends indicate damage where the separator has combusted and fragmented, causing the carbon material to detach from the aluminium current collector.

Contrary to similar studies on Li-ion batteries, the X-ray CT images of the failed supercapacitors do not exhibit common features of overheated

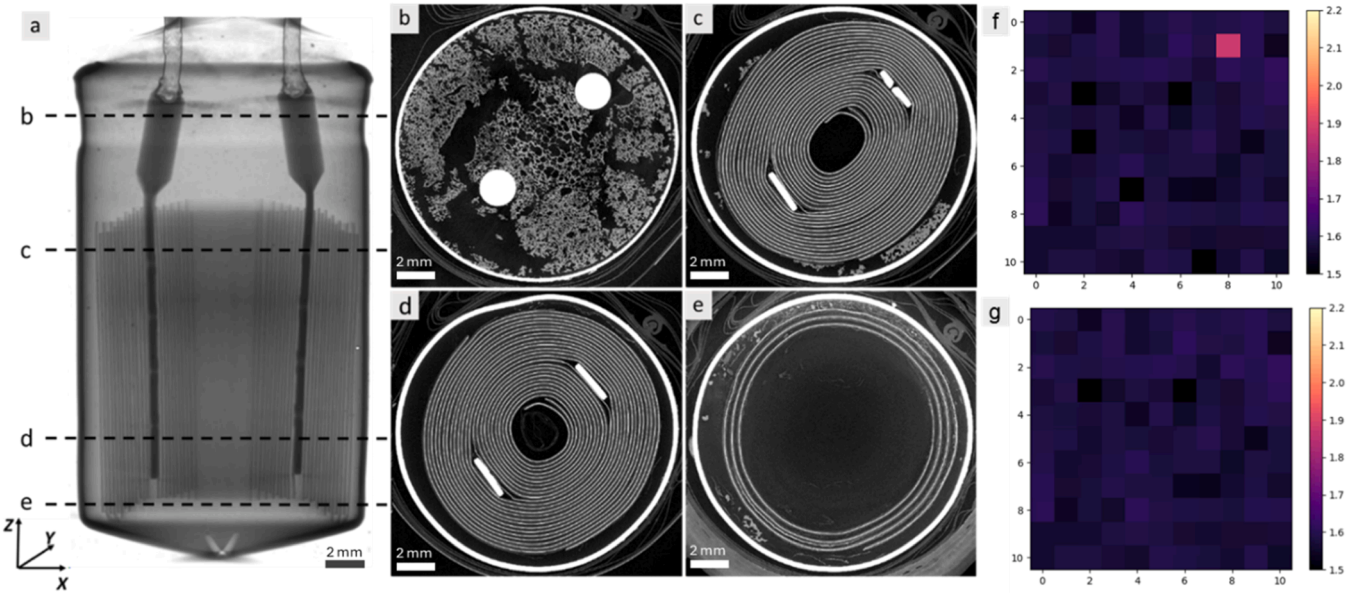

Fig. 4. Over-Heated, Post-mortem characterisation. X-ray CT images of a) overheated cell OH_4 including orthoslices in the XY plane throughout the length of the cell (b, c, d and e). Raman maps of the electrode surfaces, showing the D/G intensity ratio for the a) positive and b) negative electrode. (Raman map colour scales consistent with Fig. 1).

Li-ion cells. For instance, metallic globule formation, typically observed in Li-ion battery failures due to thermal runaway processes, involves the melting or partial melting of electrode current collectors. Despite the distorted shape of the failed supercapacitors, neither the outer casing nor the electrodes showed any signs of melting, nor the formation of globules or dendritic structures. This indicates that the internal temperatures did not exceed the melting point of aluminium (660 °C). This inference is supported by the maximum temperature of 320 °C recorded by the thermocouples, which is in stark contrast to the over 1000 °C temperatures (capable of melting the copper components of battery cells) recorded in similar failure tests on Li-ion batteries [29].

Furthermore, the differences in the temperature profiles observed during the failure of the supercapacitor devices in this study, as well as those reported in Li-ion battery literature, highlight a key distinction between the overheating failures of EDLC supercapacitors and Li-ion batteries: the process of thermal runaway. Thermal runaway, a characteristic feature of Li-ion battery failures, occurs when the cell's temperature escalates suddenly and uncontrollably due to various internal chemical reactions. In contrast, the thermal data plot shown in Fig. 2 for the EDLC supercapacitors does not exhibit any rapid temperature ramps; instead, it increases steadily until plateauing at a maximum of around 350 °C. This behaviour can be attributed to the direct effects of the external heaters rather than any exothermic reactions occurring within the cell chemistry.

This distinction is critical in applications where multiple electrochemical cells are installed in close proximity; the thermal runaway effect of a single failed cell poses a significant risk of initiating a chain of failures in nearby cells. The absence of thermal runaway, and the lack of additional heating effects created by the failure of the EDLC supercapacitors in this study suggests that these cells pose a lower risk of triggering a series of failures compared to Li-ion batteries.

The absence of any self-heating processes (thermal runaway), and consequently the relatively lower temperatures compared to Li-ion battery overheating failures, allowed for materials analysis to highlight the impact of high-temperatures within the EDLCs on the high surface area, amorphous active carbon material of the electrode surface. Since the aluminium current collector's melting point was not reached, the electrode coil was not destroyed, and remained relatively structurally intact, although it was more brittle than that of the pristine electrodes and exhibited significant delamination and other material losses. The surface was visually examined using SEM images presented in Figure SI-8.

The impacts of the high temperatures on the material structure, morphology, and therefore the potential capacity of the cell was more clearly identified through Raman spectroscopy. The Raman maps illustrated in Fig. 4f-g of the positive and negative electrodes underscore the considerable damage resulting from the overheating abuse tests. Both electrodes exhibit similar levels of damage, with a D/G intensity ratio of around 1.56 for the positive and 1.58 for the negative, indicating a substantial reduction compared to the pristine map (1.9). The uniformity observed on individual electrodes supports the SEM and X-ray CT results which revealed a lack of distinction between the electrodes. This can be attributed to the nature of the heating test, where the temperature emanates uniformly from the external heaters inwards, causing a distribution of damage across the entire cell.

Despite the notable variations in the D/G intensity ratio, the Raman maps of the over-heated cell maintain a similar level of non-uniformity across the electrode surface as the pristine map. This lack of homogeneity can be ascribed to the material loss induced by high temperatures, which covered the electrode surface with a very fine powdery carbon material, thereby impacting any long-range order that may have developed during heating. The drastically lower D/G intensity ratio when compared to the pristine map in Fig. 1 indicates that high temperatures caused a significant reduction in the electrode surface areas. The single spot in the map of the positive electrode (Fig. 4f), with a higher D/G ratio than the rest of the sample of 1.88, is considered an outlier and likely a result of impurities or contaminants to the sample surface.

3.2. *Overcharging*

Electrical issues such as failures in battery management systems, errors in charging equipment, or inadequate system designs, can periodically lead to cell overcharge or overdischarge. Overcharge is a type of failure that occurs when the charge current forces the cell voltage to exceed the cell's nominal maximum working voltage. However, despite the potential for failure, as presented by existing battery literature, the impact of overcharging on the capacity fading behaviour of

supercapacitors remains poorly documented and understudied.

Overcharging abuse tests were conducted on eight cells (OC_1 through OC_8) that were subjected to a constant current input of 4.2 A for an extended period without a voltage limit. Fig. 5 displays the electrochemical and thermal response of overcharged - Cell 1 (OC_1) under these conditions.

Initially, the current application caused the cell voltage to rapidly exceed its rated 3 V, peaking at 4.7 V and inducing a significant temperature rise. As the temperature continued to climb, the voltage gradually decreased until a sharp drop in temperature (t = 143 s) was recorded by thermocouple T1. (Fig. 5b) This indicated the release of vaporised electrolyte through venting, which corresponded to the emission of thick, grey-coloured smoke from the cell.

After the venting process, the temperature rapidly increased due to continued current application for a brief period, followed by a slight drop around t = 200 s. This temperature decrease corresponds to a brief reduction in applied current caused by a sudden voltage surge. The surge was likely caused by significant increased resistance within the cell, driven by Joule heating effects (raising the resistance in the pins and their contact points with the electrodes) and the vaporisation of electrolyte, all contributing to a sharp rise in apparent voltage. The data shows the voltage reaching the potentiostat's maximum recordable value of 12 V, but this is considered a measurement artifact due to current passing through a high-resistance system rather than the actual cell voltage exceeding this limit. As the voltage spike reached the potentiostat's physical limits, the current that could be applied to the cell was consequently restricted. After a 22-second interruption, the voltage dropped, and the system resumed applying a steady current of 4.2 A. Although the voltage did not record a drop completely to 0 V, which can be ascribed to the limits in the rate of data acquisition and the continued application of current, this can still be attributed to the occurrence of an internal short circuit caused by the breakdown of the separator, as previously described in the overheating section. Although the external cell temperature remained below the 260 °C threshold where TGA analysis of the separator (Figure SI - 9) indicated significant mass loss, the internal cell temperature likely surpassed these readings, creating conditions more conducive to separator failure. These processes were directly followed by a rapid temperature increase, thereby attributed to the reapplication of current and the sudden high-current event caused by the internal short.

Following the shorting event, the voltage profile showed significant fluctuations, with several voltage spikes accompanied by relatively constant temperature readings with minor variations correlating with periodic voltage oscillations. These behaviours are attributed to the continual application of current and the movement of components within the cell. After a period of inactivity, the applied current was discontinued, leading to an abrupt decrease in cell voltage from 1.3 V to 0 V, clearly indicating that the cell's capacity and functionality were destroyed. The electrochemical and thermal data for the two additional overcharged cells, OC_2 and OC_3, that exhibited comparable trends and are illustrated in Figure SI - 10

None of the first three overcharges experiments resulted in a catastrophic failure such as uncontrolled cell ruptures or fires. This can be attributed to the successful application of the cell's safety vent. However, further overcharge testing demonstrated that similar to overheating the process of overcharging can lead to explosive failures. In these instances, akin to the overheated cells, the cells expelled the rubber cap from the top and violently ejected the internal components. The cells OC_4 – OC_8 consistently demonstrated this as they each exploded during the test, despite equivalent conditions.

The electrochemical and thermal data in Fig. 6 show that both exploded cell OC_4 and cell OC_1 exhibited similar behaviour in the initial stages of overcharge testing, with both charging to nearly 5 V before a gradual voltage drop. The key difference emerged around 140 s when the non-exploded cells vented, releasing high pressure gasses from the high temperature cell and preventing catastrophic failure by allowing vaporised electrolyte to escape. In contrast, the exploded cells failed to vent, resulting in rupture, ejection of internal materials and cell destruction, underscoring the vent's critical role in averting such failures.

While the explosive failure of these cells clearly poses significant hazards due to the violent nature of their failure, the cells that did not rupture also present serious risks. These cells avoided explosive failure by venting, releasing hot, highly flammable vaporised electrolyte. Furthermore, the temperatures recorded for these cells were significantly higher than those of the exploded cells reaching over 300 °C, as they continued receiving current and retained more combustible material for a longer duration. These cells reached temperatures comparable with the maximum recorded in the overheating tests, suggesting that the peak temperature stabilises through radiative heat dissipation, consistent with the thermodynamic principle of detailed balance. Whilst not causing direct catastrophic failure, this prolonged exposure significantly increases the risk of inducing failure in adjacent cells or worsening preexisting hazardous conditions.

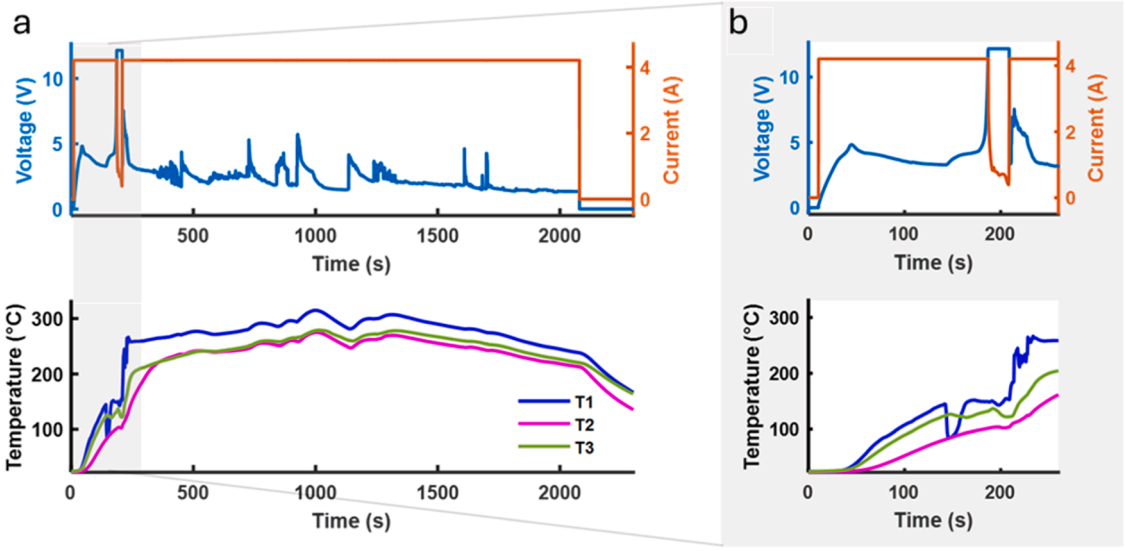

Fig. 5. Overcharging cell OC_1. Electrochemical and thermal response during overcharging at 4.2 A for an extended period of time from t = 0 s to a) t = 2300 s (full duration) and b) t = 260 s. The top plots display voltage (V, blue) and current (A, orange) profiles, while the bottom plot presents thermocouple data.

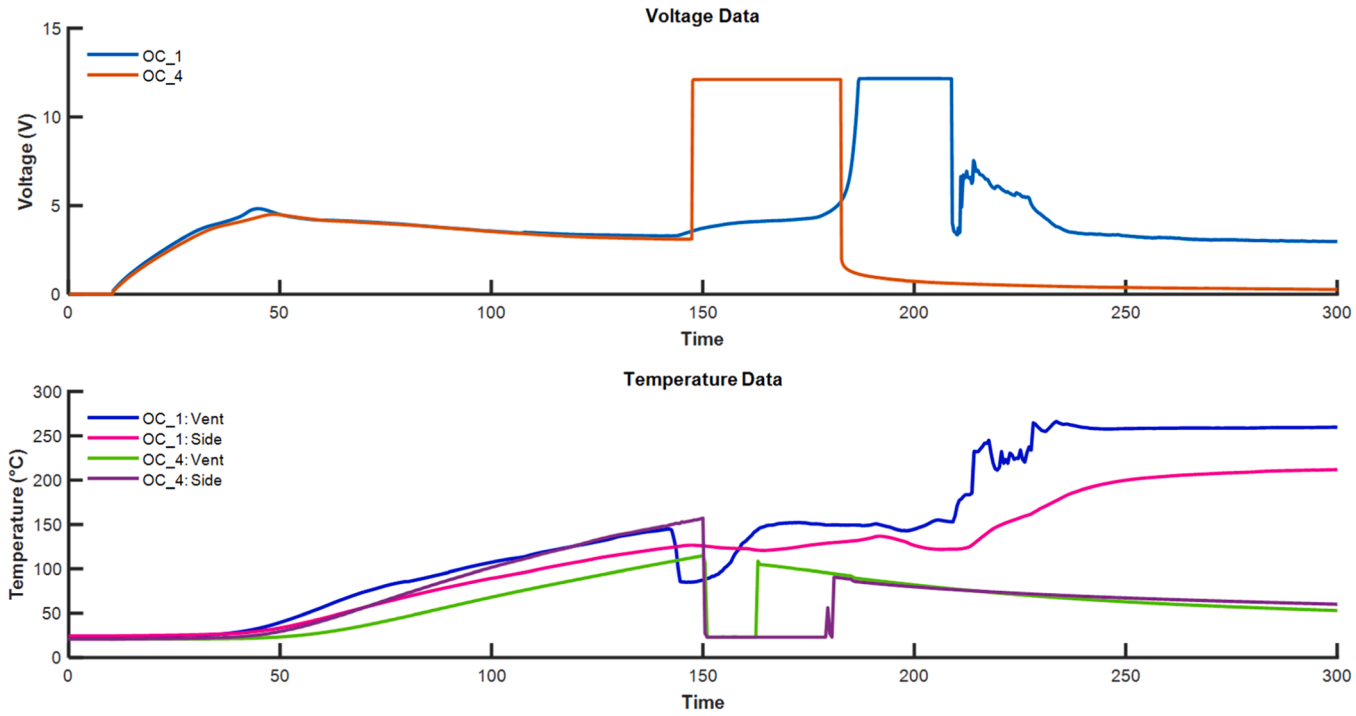

Fig. 6. Overcharging cells OC_1 and OC_4. Electrochemical and thermal response during overcharging at 4.2 A over this initial 300 s. The Top plot displays voltage profiles of OC_1 (Blue) and OC_4 (Orange), while the right plot presents thermocouple data for the vents and sides cells OC_1 and OC_4, for the initial 300 s.

The explosive failures of cells OC_4 - OC_8 made it impossible to use X-ray CT imaging to visualise the changes caused by the overcharging process to the cell structure. Therefore, Fig. 7 illustrates the effects of overcharging on the non-exploded cell OC_1.

The rubber stopper at the top of cell OC_1 disintegrated due to high temperatures caused by overcharging, resulting in limited structural integrity that caused it to crumble upon handling (Fig. 7b). Examination of the coil revealed that most damage was concentrated in the centre (Fig. 7c), evidenced by the accumulation of detached electrode material, warping of the current collector, as well as fractures and deformations of the electrodes. This phenomenon likely occurs because the coil has more room to collapse inward, causing the electrode layers to fray at these points compared to the tightly packed structure of the remaining coil. This is corroborated by the significant fraying observed on the outer layer of the coil (Fig. 7d). However, it is challenging to determine whether the material separation is primarily concentrated in the centre of the coil and around the pins, or if these areas simply provide better visibility of the material detachment due to being less tightly wound.

Further observations indicate irregular and non-uniform spacing between electrode layers and the complete disintegration of the separator structure within the coil. The pins acted as hotspots due to concentrated current flow and caused a significantly larger proportion of

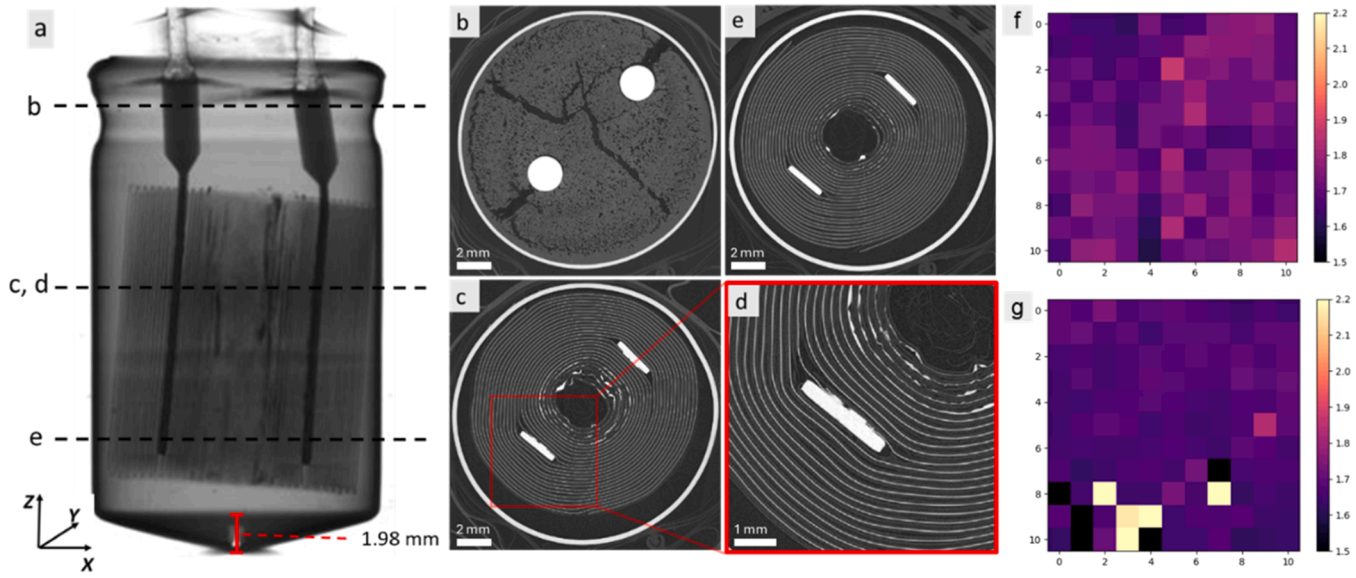

Fig. 7. Overcharged cell post-Mortem Characterisation. X-ray CT images of a) overcharged cell OC_1 including orthoslices in the XY plane throughout the length of the cell (b, c, d and e). Raman map of the overcharged cell OC_1 electrode surface, showing the D/G intensity ratio for the f) positive and g) negative electrode. (Raman map colour scale is consistent with those in Figs. 1 and 4).

material detachment from the current collector in areas close to the pin location. This pattern of damage was consistent across all overcharged cells, indicating a well-established failure behaviour for this system. The localised areas of damage observed here contrasts the more evenly distributed damage observed in the overheated cells.

Disassembly of the overcharged cells (Figure SI - 11), revealed that most of the material had combusted and detached from the coil, resulting in a significant amount of loose powder inside the cell casing (Figure SI - 11c). The electrodes in all three cells were fragile and flaky, with substantial quantities of carbonaceous material easily expelled. The separator was also burned and disintegrated, as confirmed by unwinding the coil. Notably, the positive electrode exhibited more damage than the negative in all three cells. While the negative electrode showed signs of material detachment, the positive electrode had significantly more material loss, exposing large areas of the current collector (Figure SI - 12). SEM images, presented in Figure SI - 13, corroborated this, showing that regions on the positive electrode near the pins, where the current density would have been greatest, exhibited the most significant material loss. Additionally, hair-like remnants of the incinerated separator were observed among the particles near the positive pin, while areas further from the pins retained more electrode material attached to the current collector and less separator remains, indicating that the application of current was a driving force for the deposition of this material.

The Raman maps presented in Fig. 7f and g illustrate the formation of a passivation layer on the surface of the carbonaceous electrode materials, indicated via a general decrease in the average D/G intensity ratio and an increase in homogeneity across the mapped region. The maps reveal an unequal level of damage between the electrode surfaces, which appears to contrast with the SEM and visual observations. The positive electrode shows a more amorphous and disordered surface with a higher average D/G intensity ratio than the negative electrode. While both exhibit lower D/G ratios than in their pristine state, the variability of the positive electrode's D/G ratio indicates a non-homogeneity that aligns more closely with the pristine electrode than the negative. This discrepancy can be attributed to the significant delamination of the surface layers of the positive electrode, exposing the underlying, less damaged bulk material. This observation further supports the conclusion that the positive electrode experienced a higher level of damage.

4. Discussion

Although supercapacitors are often considered less prone to catastrophic failure than batteries, our findings show that EDLC supercapacitors are susceptible to failure modes which can result in energetic and explosive cell failures when exposed to abusive conditions. Both abuse methods examined in this study induced distinct failure effects and yet followed a common failure mechanism driven by the high temperatures experienced by the cells. Regardless of the heating method, whether externally through overheating or internally via applied current through overcharging, the cells exhibited comparable behaviour, with the most notable exception being the distribution of damage within the cells: overheating caused a more widely distributed spread of damage, while overcharging led to more localised effects centred around the pins and created a disparity in the extent of damage between the electrodes.

Elevated temperatures were identified as the primary factor leading to cell degradation and failure. This process involved the deterioration of electrode surfaces and significant delamination of electrode material, particularly in areas with extra space where the dislodged material could accumulate. Additionally, temperatures exceeding 150 °C resulted in the breakdown and eventual destruction of the separator, causing internal short circuits, effectively destroying the functionality of the cells. Post-mortem X-ray CT imaging confirmed these observations revealing that the separators had been destroyed. In addition, overheated cells displayed loose material along the outer edge of the electrode coil (Fig. 4c) and overcharged cells showed damage surrounding and between the pins (Figure SI - 7d).

The most significant effect of this thermal failure mode was attributed to the vaporisation of the acetonitrile-based electrolyte, leading to a substantial pressure build-up. This condition led to either gradual venting or sudden cell rupture, both of which release hazardous gases and toxic decomposition byproducts. In many of the overcharging and overheating tests, the pressure accumulation was managed through the gassing process facilitated by the vent on the base of the cell. However, concerning vent failure rates of 40 % and 62.5 % were observed in the overheated and overcharged cells respectively, indicating a significant safety risk. Whilst these failures might be attributed to manufacturing defects, none were identified during initial observations or X-ray CT scans prior to testing.

The existing literature on this topic is notably sparse, with the only comparable study being that of Hund et al. [20], which discussed the release of flammable and toxic gases as a result of overheating and overcharging conditions. However, the study did not characterise the effects of abuse on the cells, nor did it address specific failure modes. Our study provides post-mortem characterisation and analysis that offers a full cell understanding of the failure effects. A key technique in our research was the use of three-dimensional imaging methods, such as X-ray CT, which provided a more comprehensive understanding of the effects of abuse on these cells by visualising the internal structures before post-mortem tear-down analysis.

In contrast to the extensive body of research on abuse testing and failure modes of Li-ion batteries, which has identified several distinctive features such as thermal runaway, metallic globules, vent blocking, fires, and explosions, our study highlights the absence of many of these phenomena in the failure of EDLCs. Most notably, thermal runaway—a process in which exothermic reactions within the battery cause a rapid increase in temperature, and often lead to explosive failures[3,30]. The cells investigated in this study exhibited stable heating trends without significant temperature spikes or undergoing self-heating, indicating the lack of a thermal runaway process. We attribute this to the simpler chemistry of EDLCs, which lacks the components necessary for such exothermic reactions.

5. Conclusion

While EDLCs are generally considered safer than Li-ion batteries, we can conclude that they are not entirely risk-free. The observed explosive failures, though less severe than typical Li-ion battery explosions, still present hazards, such as high temperatures, shrapnel, and released gases, which can endanger individuals and nearby devices. Furthermore, the structural vent designed to mitigate some explosive failures, functions by releasing the built-up flammable gases, a process that can significantly increase the risk of igniting or exacerbating a pre-existing fire.

This investigation therefore underscores the vulnerability of supercapacitors under abuse conditions showing distinct differences from Li-ion batteries which typically exhibit thermal runaway. Instead, it was observed that the thermal failure of supercapacitors involves the release of gases, fires, and sometimes explosions, under similar conditions. The inherent properties of EDLCs reduce the risk of catastrophic failures, but future research should consider a wider range of abusive conditions as well as different supercapacitor chemistries and geometries such as pseudo- and hybrid- capacitors, where additional chemical reactions could introduce greater complexity and potential hazards. Additionally, understanding supercapacitor failure within their application context is crucial, as this study demonstrates their potential to create and propagate the conditions necessary to induce failures in adjacent cells or exacerbate ongoing failure cascades.

CRediT authorship contribution statement

Katrina Mazloomian: Writing – review & editing, Writing – original

draft, Methodology, Investigation. **Thomas R. Dore:** Writing – review & editing, Writing – original draft, Methodology, Investigation, Formal analysis, Data curation. **Mark Buckwell:** Writing – review & editing, Methodology, Investigation. **Liam Bird:** Writing – review & editing, Methodology, Investigation. **Paul R. Shearing:** Writing – review & editing, Methodology, Funding acquisition. **Thomas S. Miller:** Writing – review & editing, Supervision, Resources, Project administration, Methodology, Funding acquisition, Conceptualization.

Declaration of competing interest

The authors declare the following financial interests/personal relationships which may be considered as potential competing interests:

T S Miller reports financial support was provided by The Faraday Institution. Paul Shearing reports financial support was provided by Royal Academy of Engineering. If there are other authors, they declare that they have no known competing financial interests or personal relationships that could have appeared to influence the work reported in this paper.

Acknowledgements

The present research has been supported by the Faraday Institution (EP/S003053/1), LiSTAR (FIRG014 FIRG058), Safebatt (FIRG028, FIRG059) and Nextrode (FIRG066) projects. PRS acknowledges The Royal Academy of Engineering (CiET1718/59). KM acknowledges support from the UCL H. Walter Stern Scholarship.

Supplementary materials

Supplementary material associated with this article can be found, in the online version, at doi:10.1016/j.ensm.2025.104115.

References

[1] J. Partridge, D.I. Abouelamaimen, The role of Supercapacitors in regenerative braking systems, Energies. (Basel) 12 (2019).
[2] A. Kumar, S. Ibraheem, R.K. Gupta, T.A. Nguyen, G. Yasin, H. Song, T.A. Nguyen, G. Yasin, N.B. Singh, R.K. Gupta, Chapter 21 - battery-supercapacitor hybrid systems: an introduction. Nanotechnology in the Automotive Industry, Elsevier, 2022, pp. 453–458, https://doi.org/10.1016/B978-0-323-90524-4.00021-9.
[3] D. Patel, J.B. Robinson, S. Ball, D.J.L. Brett, P.R. Shearing, Thermal runaway of a Li-ion battery studied by combined ARC and multi-length scale X-ray CT, J. Electrochem. Soc. 167 (2020) 090511.
[4] M. Fransson, et al., Exploring thermal runaway propagation in Li-ion batteries through high-speed X-ray imaging and thermal analysis: impact of cell chemistry and electrical connections, J. Power. Sources. 617 (2024) 234916.
[5] A. Fordham, et al., Investigating the performance and safety of Li-Ion cylindrical cells using acoustic emission and machine learning analysis, J. Electrochem. Soc. 171 (2024) 70521.
[6] F. Larsson, B.-E. Mellander, Abuse by external heating, overcharge and short circuiting of commercial lithium-ion battery cells, J. Electrochem. Soc. 161 (2014) A1611.
[7] X. Feng, et al., Thermal runaway mechanism of lithium ion battery for electric vehicles: a review, Energy Storage Mater. 10 (2018) 246–267.
[8] C. Wu, J. Sun, C. Zhu, Y. Ge, Y. Zhao, Research on overcharge and Overdischarge effect on lithium-ion batteries, in: 2015 IEEE Vehicle Power and Propulsion Conference (VPPC), 2015, pp. 1–6, https://doi.org/10.1109/VPPC.2015.7353006.
[9] V. Ruiz, et al., A review of international abuse testing standards and regulations for lithium ion batteries in electric and hybrid electric vehicles, Renew. Sustain. Energy Rev. 81 (2018) 1427–1452.
[10] D.H. Doughty, SAE J2464" EV & HEV rechargeable energy storage system (RESS) safety and abuse testing procedure, SAE Int (2010).
[11] A. Stein, et al., Thermal electrical tests for battery safety standardization, Energies. (Basel) 15 (2022) 7930.
[12] P. Azaïs, P. Kuntz, Standards and safety, Li-ion batteries (2022) 317–350.
[13] Y. Chen, et al., A review of lithium-ion battery safety concerns: the issues, strategies, and testing standards, J. Energy Chem. 59 (2021) 83–99.
[14] K. Mazloomian, H.J. Lancaster, C.A. Howard, P.R. Shearing, T.S. Miller, Supercapacitor degradation: understanding mechanisms of cycling-induced deterioration and failure of a Pseudocapacitor, Batter. Supercaps. 6 (2023) e202300214.
[15] A.M. Bittner, et al., Ageing of electrochemical double layer capacitors, J. Power. Sources. 203 (2012) 262–273.
[16] P. Ratajczak, K. Jurewicz, F. Béguin, Factors contributing to ageing of high voltage carbon/carbon supercapacitors in salt aqueous electrolyte, J. Appl. Electrochem. 44 (2014) 475–480.
[17] G. Walden, J. Stepan, C. Mikolajczak, Safety considerations when designing portable electronics with Electric Double-Layer capacitors (Supercapacitors), in: *2011 IEEE Symposium on Product Compliance Engineering Proceedings* 1–5, 2011, https://doi.org/10.1109/PSES.2011.6088259.
[18] O. Bolufawi, A. Shellikeri, J.P. Zheng, Lithium-Ion capacitor safety testing for commercial application, Batteries. (Basel) 5 (2019).
[19] M. Wu, C. Zhang, C. Yang, Z. An, J. Xu, Over-heating triggered thermal runaway characteristic of lithium ion hybrid supercapacitor based lithium nickel cobalt manganate oxide/activated carbon cathode and hard carbon anode, Solid. State Ion. 377 (2022) 115883.
[20] Hund, T.D., Romero, J.A., Clark, N.H. & Johnson, D.I. *Abuse testing results form symmetric Carbon/Carbon acetonitrile electrolyte Supercapacitors using over voltage and over temperature environments*. (2006).
[21] M. Al Sakka, H. Gualous, J. Van Mierlo, H Culcu, Thermal modeling and heat management of supercapacitor modules for vehicle applications, J. Power. Sources. 194 (2009) 581–587.
[22] V.V.N. Obreja, A. Dinescu, A.C. Obreja, Activated carbon based electrodes in commercial supercapacitors and their performance, Int. Rev. Electr. Eng 5 (2010) 272–281.
[23] A.C. Ferrari, J. Robertson, Interpretation of Raman spectra of disordered and amorphous carbon, Phys. Rev. B 61 (2000) 14095.
[24] Xiong, G., Kundu, A. & Fisher, T. Influence of temperature on Supercapacitor performance. in 71–114 (2015). doi:10.1007/978-3-319-20242-6_4.
[25] E. Pameté, et al., The Many Deaths of Supercapacitors: degradation, Aging, and performance fading, Adv. Energy Mater. 13 (2023).
[26] A. Bothe, A. Balducci, The impact of the thermal stability of non-conventional electrolytes on the behavior of high voltage electrochemical capacitors operating at 60°C, Electrochim. Acta 374 (2021) 137919.
[27] Sigma-Aldrich. Acetonitrile - SAFETY DATA SHEET. https://www.sigmaaldrich.com/GB/en/sds/sial/271004.
[28] X. Lai, et al., Mechanism, modeling, detection, and prevention of the internal short circuit in lithium-ion batteries: recent advances and perspectives, Energy Storage Mater. 35 (2021) 470–499.
[29] A.W. Golubkov, et al., Thermal runaway of commercial 18650 Li-ion batteries with LFP and NCA cathodes – impact of state of charge and overcharge, RSC. Adv. 5 (2015) 57171–57186.
[30] D.P. Finegan, et al., The battery failure databank: insights from an open-access database of thermal runaway behaviors of Li-ion cells and a resource for benchmarking risks, J. Power. Sources. 597 (2024) 234106.